Ocean Sci., 20, 1423–1440, 2024
https://doi.org/10.5194/os-20-1423-2024

Ocean Science Open Access EGU

Alkalinity sources in the Dutch Wadden Sea

Mona Norbisrath[1,2,a], **Justus E. E. van Beusekom**[1], **and Helmuth Thomas**[1,2]

[1]Institute of Carbon Cycles, Helmholtz-Zentrum Hereon, 21502 Geesthacht, Germany
[2]Institute for Chemistry and Biology of the Marine Environment (ICBM), Carl von Ossietzky University of Oldenburg, 26129 Oldenburg, Germany
[a]now at: Department of Marine Chemistry and Geochemistry, Woods Hole Oceanographic Institution, Woods Hole, MA 02543, USA

Correspondence: Mona Norbisrath (mona.norbisrath@gmail.com)

Received: 3 November 2023 – Discussion started: 9 November 2023
Revised: 27 August 2024 – Accepted: 30 August 2024 – Published: 30 October 2024

Abstract. Total alkalinity (TA) is an important chemical property that plays a decisive role in the oceanic buffering capacity with respect to CO_2. TA is mainly generated by weathering on land as well as by various anaerobic metabolic processes in the water and sediments. The Wadden Sea, located in the southern North Sea, is hypothesized to be a source of TA for the North Sea, but quantifications are scarce. This study shows observations of TA, dissolved inorganic carbon (DIC), and nutrients in the Dutch Wadden Sea in May 2019. Surface samples were taken along several transects in order to investigate spatial distribution patterns and compare them with data from the late 1980s. A tidal cycle was sampled to further shed light on TA generation and potential TA sources. We identified the Dutch Wadden Sea as a source of TA and estimated an export of 6.6 Mmol TA per tide to the North Sea. TA was generated in the sediments, with deep pore water flow during low tide enriching the surface water. A combination of anaerobic processes and $CaCO_3$ dissolution were potential TA sources in the sediments. We deduce that seasonality and the associated nitrate availability specifically influence TA generation by denitrification, which is low in spring and summer.

1 Introduction

As the regulator of the ocean carbon dioxide (CO_2) sink, total alkalinity (TA) is of increasing scientific interest and has been investigated worldwide in the so-called "Anthropocene" (Abril and Frankignoulle, 2001; Bozec et al., 2005; Chen and Wang, 1999; Dickson, 1981; Middelburg et al., 2020; Norbisrath et al., 2022; Renforth and Henderson, 2017; Thomas et al., 2004, 2009; Sabine et al., 2004). The Anthropocene describes the current era of our planet, during which environmental changes, driven by humans, have become identifiable in geological records (Zalasiewicz et al., 2010; Crutzen, 2002). One of the most threatening changes with respect to our climate is the anthropogenic increase in atmospheric greenhouse gases (GHGs), such as CO_2. To counteract the increasing atmospheric CO_2 concentrations and ongoing climate warming, a combination of several pathways is needed. In addition to a strict reduction in CO_2 emissions, net-negative emissions are also required; to achieve the latter, atmospheric CO_2 must be captured and stored, either on land or in the ocean (e.g., Keith et al., 2006; Matthews and Caldeira, 2008; Zhang et al., 2022). The climate and the increasing atmospheric CO_2 content is also naturally regulated by the open ocean, and around a quarter of the global anthropogenic CO_2 emissions are already removed by it (Friedlingstein et al., 2022). The carbon storage capacity of the North Sea is an important atmospheric CO_2 sink, as it exports the absorbed CO_2 to the deep layers of the Atlantic Ocean where it is then stored on longer timescales (Borges et al., 2005; Bozec et al., 2005; Burt et al., 2016; Brenner et al., 2016; Hu and Cai, 2011; Schwichtenberg et al., 2020; Thomas et al., 2004, 2009). Two important aspects of oceanic climate regulation are the oceanic circulation and TA. TA, primarily consisting of bicarbonate and carbonate, is generated by chemical rock weathering (Suchet and Probst, 1993; Meybeck, 1987; Berner et al., 1983) as well as in various stoichiometries by calcium carbonate ($CaCO_3$) dissolution and

anaerobic metabolic processes, such as denitrification, which is the reduction process of nitrate to dinitrogen gas in the nitrogen cycle (Hu and Cai, 2011; Wolf-Gladrow et al., 2007; Chen and Wang, 1999; Brewer and Goldman, 1976). As TA, CO_2 uptake, and CO_2 export to the deep ocean are mainly disentangled in the open ocean, TA and the oceanic circulation interact closely in highly active and shallow-ocean areas, such coastal zones and continental and marginal shelves.

In these shallow areas, TA is susceptible to changes due to various metabolic processes and the influence of adjacent zones like rivers, estuaries, marshes, and tidal flats (e.g., Norbisrath et al., 2022, 2023; Wang et al., 2016; Voynova et al., 2019). A previous study by Norbisrath et al. (2022) showed that an enhanced riverine metabolic alkalinity would lead to increasing CO_2 absorption in the coastal zones of the North Sea, highlighting the need to further investigate TA regulation in adjacent zones of coastal oceans.

Coastal zones, which are the direct interface between most (if not all) compartments of the Earth system (i.e., atmospheric, terrestrial, aquatic, and oceanic) and human societies, appear particularly vulnerable to environmental and climate change (Glavovic et al., 2015). This holds true for the Wadden Sea, the shallow coastal sea along an approximately 500 km coastline of the Netherlands, Germany, and Denmark, in the southern North Sea, which has been declared a UNESCO world natural heritage site since 2009. Most of the Wadden Sea is located between protective barrier islands and the mainland, making it the world's largest uninterrupted stretch of tidal flats with multiple tidal inlets (Fig. 1). Due to the region's topography, the Wadden Sea is a highly dynamic ecosystem with influences from the mainland and the North Sea (Hoppema, 1993; Postma, 1954; van Raaphorst and van der Veer, 1990). Driving forces of the biogeochemical dynamics in the Wadden Sea are nutrient imports by rivers and high suspended particulate matter (SPM) and organic matter (OM) imports from the North Sea (van Beusekom et al., 2019, 2012; Postma, 1954). Physical sources of variability in the Wadden Sea are ocean-driven wind, waves, and tidal currents as well as the counterclockwise circulation of the North Sea (Elias et al., 2012). A large tidal amplitude and currents in conjunction with shallow water depths allow for vertical water column mixing and an exchange between the pelagic and benthic realms, including deep pore water exchange (Røy et al., 2008). The strong tidal currents also impact the biogeochemistry of the North Sea (Postma, 1954), as they cause an exchange of water between the North Sea and the Wadden Sea and play an important role in the import of particulate matter from the North Sea (Burchard et al., 2008).

Previous studies have identified the Wadden Sea as a TA source for the North Sea, with a loading of between 39 $\mathrm{Gmol\,yr^{-1}}$ (Schwichtenberg et al., 2020) and 73 $\mathrm{Gmol\,yr^{-1}}$ (Thomas et al., 2009). Both of these prior publications suggested that the entire Wadden Sea is one of the most important TA sources impacting the carbon storage capacity of the North Sea. Burt et al. (2016) highlighted the importance of coastal TA production with respect to regulating the buffer system in the North Sea and suggested denitrification as the major TA source. Due to the strong connection between the North Sea and the Wadden Sea, a better understanding of TA generation in the latter is required. Here, we focus on the Dutch Wadden Sea, which has been well-studied during the past decades (Hoppema, 1990, 1991, 1993; De Jonge et al., 1993; Elias et al., 2012; Ridderinkhof et al., 1990; Postma, 1954; van Beusekom et al., 2019; Schwichtenberg et al., 2017). In particular, in the late 1980s, Hoppema (1990, 1993) observed the spatiotemporal variability in TA in the month of May; we compare those findings with our observed transect data to detect potential differences over the last 30 years. In addition, we further discussed potential TA sources in the Dutch Wadden Sea.

2 Methods

2.1 Study site and sampling

This study is based on samples collected on a research cruise (no. LP20190515) on RV *Ludwig Prandtl* in the Dutch Wadden Sea (Frisian Islands) in May 2019 (Fig. 1). We collected water samples in the Wadden Sea starting at Harlingen and traveling along the following path: through the Vlie Inlet along the islands of Vlieland and Terschelling, through the Ameland Inlet to Ameland Island, via the Frisian Inlet to Lauwersoog, and around Schiermonnikoog Island via the Ems-Dollard Inlet to Emden. In addition, we sampled half a tidal cycle during ebb tide (from high tide to low tide) on 21 May 2019 (Table B2). To set the range of ebb tide data, we also sampled half a tidal cycle during flood tide (from low tide to high tide) on 23 May 2019 for comparison. Both of the half tidal cycles were sampled each day using an anchor station in the waterway on the western side of Ameland in the Ameland Inlet.

Nearly every 30 min, we collected discrete surface (1.2 m depth) water samples with a bypass from the onboard flow-through FerryBox system, which also provided essential physical parameters, such as salinity, with an accuracy of 0.02 PSU (practical salinity units) and temperature with an accuracy of 0.1 °C (Petersen et al., 2011). The FerryBox was cleaned and checked prior to the cruise, and salinity was occasionally checked using discrete samples; this workflow is considered sufficient for gradients in near-shore investigations (Yoana Voynova, personal communication, 2024). We complemented our salinity and temperature data with data from three Rijkswaterstaat stations (Dantziggat, Terschelling 10, and Vliestroom; Table B3), which were close to our stations.

For TA and dissolved inorganic carbon (DIC) measurements, we sampled water with overflow into 300 mL BOD (biological oxygen demand) bottles and preserved it with 300 µL of saturated mercury chloride solution ($HgCl_2$) to

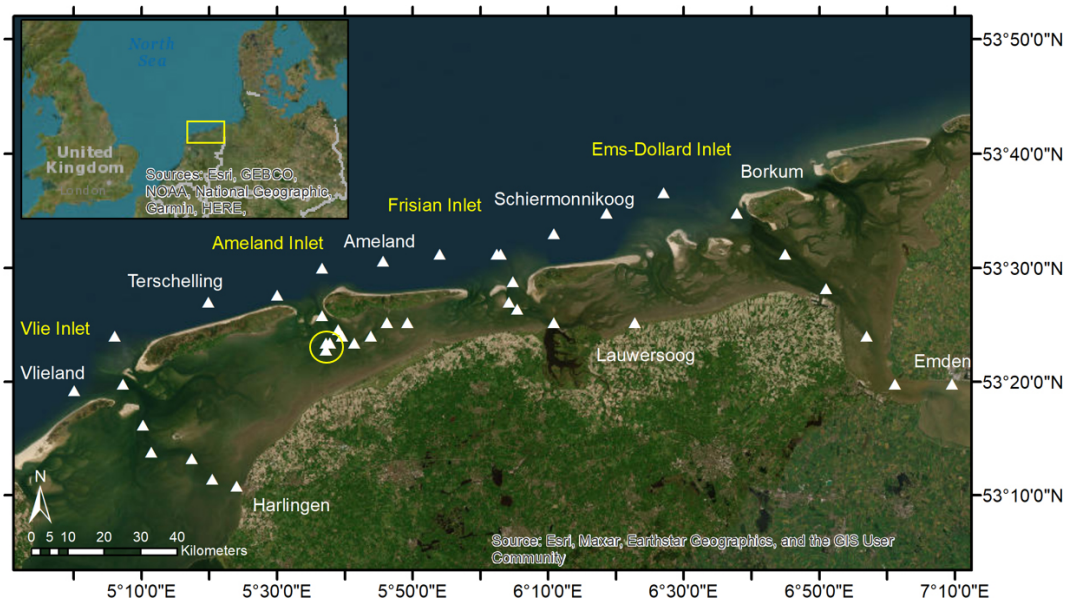

Figure 1. Sampling site in the Dutch Wadden Sea. The sampling stations around the Frisian Islands in May 2019 are visualized using white triangles. The yellow circle highlights the anchor stations used to sample the tidal cycle in the Ameland Inlet on 2 d. During the sampling day, from low tide to high tide, we had two samples that were taken slightly more to the west due to drift. The island and city names are shown in white, whereas the inlets are shown in yellow. The tidal flats and sedimentary structures are visible between the barrier islands and the mainland.

stop biological activity. Each BOD bottle was filled without air bubbles and closed using a ground-glass stopper coated in Apiezon® M grease and a plastic cap. The samples were stored in a cool, dark environment prior to analysis in the lab.

Water for nutrient samples was filtered through pre-combusted (4 h at 450 °C) GF/F filters, and the filtrate was stored frozen in three 15 mL Falcon® tubes for triplicate measurements in the lab.

To determine the total carbon (C), organic carbon (C_{org}) and nitrogen (N) concentrations in SPM, and associated C_{org} : N ratios, we used pre-combusted (4 h at 450 °C) GF/F filters; the filters were dried after sampling at 50 °C to remove all humidity and then stored frozen until measurement.

2.2 Carbon species analyses

The parallel analyses of TA and DIC were carried out in March 2020 using the MARIANDA (MARIne ANalytics and Data) VINDTA 3C (Versatile INstrument for the Determination of Total dissolved inorganic carbon and Alkalinity) instrument, which measures TA (via potentiometric titration) and DIC (via coulometric titration), both with a measurement precision of $< 2\,\mu mol\,kg^{-1}$ (Shadwick et al., 2011). Certified reference material (CRM batch no. 187), provided by Andrew G. Dickson (Scripps Institution of Oceanography), was measured before and after the samples and used to ensure a consistent calibration of both measurements.

The calcite and aragonite saturation states (Ω), the pH, and the seawater partial pressure of CO_2 (pCO_2) were computed with the CO2SYS program (Lewis and Wallace, 1998), using the measured parameters TA and DIC, salinity, temperature, silicate, and phosphate as input variables as well as the dissociation constants from Mehrbach et al. (1973), as refitted by Dickson and Millero (1987). Reported calculation uncertainties are ± 0.0062 for pH (Millero et al., 1993), ± 4.9 % for the aragonite saturation state, and ± 3.5 % for pCO_2 (Orr et al., 2018).

2.3 Nutrient analyses

The nutrients were measured with a continuous-flow automated nutrient analyzer (AA3, SEAL Analytical) and a standard colorimetric technique (Hansen and Koroleff, 2007) for nitrate (NO_3^-), nitrite (NO_2^-), phosphate (PO_4^{3-}), and silicate (Si), whereas a fluorometric method (Kérouel and Aminot, 1997) was employed for ammonium (NH_4^+) (Grasshoff et al., 2009). The nutrient samples were measured against Eurofins Scientific reference materials VKI SW4.1B (for NO_x, NO_2, and NH_4) and VKI SW4.2B (for Si and PO_4) in July 2019. The maximum standard deviations were $0.322\,\mu mol\,L^{-1}$ for NO_3^-, $0.014\,\mu mol\,L^{-1}$ for NO_2^-, $0.081\,\mu mol\,L^{-1}$ for NH_4^+, $0.014\,\mu mol\,L^{-1}$ for PO_4^{3-}, and $0.165\,\mu mol\,L^{-1}$ for Si.

For C_{org} determination, filters were acidified with 1N HCl and dried overnight to remove all inorganic carbon content. Filters were measured with a CHN (carbon–hydrogen–nitrogen) elemental analyzer (Eurovector EA 3000, HEKAtech GmbH) at the Institute of Geology, University of Ham-

burg, and calibrated against a certified acetanilide standard (IVA Analysentechnik). The standard deviations were 0.05 % for carbon and 0.005 % for nitrogen.

2.4 Data analyses

The data analyses were performed using RStudio (Version 1.3.1073, © 2009–2020 RStudio, Posit PBC; R Core Team, 2019). The linear regression Model II was performed using the "lmodel2" R package (Legendre, 2018), and the plots were created with the "ggplot2" R package (Wickham, 2016).

3 Results

3.1 Spatial parameter distribution

To investigate the spatial distribution of TA in the Dutch Wadden Sea and compare its general status with earlier studies (in particular Hoppema, 1990), we observed TA and related parameters in surface water along a transect from the coastal mainland towards the North Sea.

The temperature varied between 12 and 16 °C, with higher temperatures towards the coastal mainland (Fig. 2a). We identified two main subregions based on the salinity values: (1) the Ems-Dollard Inlet, which showed salinity values lower than 28 PSU and had a minimum value of 20.25 PSU at the most upstream station, and (2) the area around Ameland Island and the remainder of our investigated region in the Dutch Wadden Sea, which showed salinity values from 28 to 33 PSU with little variation (Fig. 2b).

The spatial transect of TA concentrations ranged from 2332 to 2517 $\mu mol\,TA\,kg^{-1}$. We observed lower concentrations on the North Sea side of the Frisian Islands, with somewhat higher concentrations around Ameland (Fig. 2c). In contrast to the North Sea side, the values were higher ($>$ 2380 $\mu mol\,TA\,kg^{-1}$) in the Wadden Sea. In the Ems-Dollard Inlet, the concentrations were even higher, with values of up to 2517 $\mu mol\,TA\,kg^{-1}$ at the most upstream station.

Silicate (Si) showed higher concentrations in the Wadden Sea and lower values towards the North Sea (Fig. A1a). The highest concentrations were observed at the coastal mainland and in the Ems-Dollard Inlet. Silicate concentrations ranged between 0.3 and 56.3 $\mu mol\,Si\,L^{-1}$. Both the calcite and aragonite saturation states (Ω) were supersaturated throughout the study region. The Ω values ranged from 2.3 to 4.6 for calcite (Fig. A1b) and from 1.4 to 2.8 for aragonite (Table B3). The highest values were observed on the North Sea side of the barrier islands, whereas the lowest values were found near Harlingen and in the Ems-Dollard Inlet. Like the calcite and aragonite saturation states, the pH values were higher in the North Sea, whereas they were lower in the Wadden Sea and near the coastal mainland (Fig. A1c). The pH values ranged from 7.86 to 8.19, with the lowest readings observed near Harlingen and in the Ems-Dollard Inlet. The nitrate (NO_3^-) concentrations fell within in a low range ($< 3\,\mu mol\,NO_3^-\,L^{-1}$) throughout the study region. Higher concentrations ($< 6\,\mu mol\,NO_3^-\,L^{-1}$) were only observed at a few stations close to land, and the maximum concentrations ($< 38\,\mu mol\,NO_3^-\,L^{-1}$) were observed in the Ems-Dollard Inlet (Fig. A1d). DIC concentrations ranged from 2097 to 2430 $\mu mol\,DIC\,kg^{-1}$ (Fig. A1e). DIC values showed a similar pattern to TA values: higher concentrations near the coastal mainland and in the Ems-Dollard Inlet and decreasing concentrations toward the North Sea, where DIC reached minimum values.

Compared with the other transects of this study region, the strong influence of the inner Ems Estuary is visible at the most upstream station in the Ems-Dollard Inlet, showing the lowest salinity values; the lowest pH and calcite saturation state values; and the highest TA, DIC, nitrate, silicate, and phosphate values. The outer side of the Vlie Inlet reflects the North Sea conditions: lower temperatures and higher salinities. The North Sea impact is also visible in the mixing plot between TA and salinity (Fig. 3). Statistically significant linear mixing behavior was observed in the transect through the Ems-Dollard Inlet ($R^2 = 0.81$) and through the Vlie Inlet ($R^2 = 0.77$), where TA concentrations decreased with increasing salinities from the mainland towards the North Sea (Fig. 3). Whereas in the Ems-Dollard Inlet mixing is dominated by riverine water with high TA concentrations, the mixing in the Vlie Inlet showed a more prominent mixing of Wadden Sea and North Sea water. The TA concentrations in the Vlie Inlet and around Ameland, both on the North Sea side (Ameland NS) and the Wadden Sea side (Ameland WS), were higher than the TA concentration computed for the salinity end-member in the Ems-Dollard Inlet, suggesting the Dutch Wadden Sea as a source of TA (Fig. 3). Both Ameland NS and Ameland WS data clearly indicated nonconservative behavior with a range of TA concentrations at near-constant salinities.

3.2 Tidal cycle

In order to (1) identify potential TA sources and (2) to quantify potential TA export to the North Sea, we observed half a tidal cycle at an anchor station in the Ameland Inlet during ebb tide. We identified patterns in several biogeochemical parameters in water leaving the tidal flats (Fig. 4, Table B1). Temperature increased from 13.25 to 14.7 °C (Fig. 4a). Salinity was constant at around 32.5 PSU (Fig. 4b), which is within the range of coastal southern North Sea water excluding admixture of local freshwater sources.

During ebb tide, TA ranged from 2387 $\mu mol\,TA\,kg^{-1}$ during high tide to 2438 $\mu mol\,TA\,kg^{-1}$ during low tide (Fig. 4c). We observed an increase of 51.6 $\mu mol\,TA\,kg^{-1}$ (ΔTA) during ebb tide (6.8 h), resulting in a TA increase of 7.6 $\mu mol\,TA\,kg^{-1}\,h^{-1}$ at the sampling location.

DIC concentrations behaved similarly to TA, with minimum values at high tide (2172 $\mu mol\,DIC\,kg^{-1}$) and max-

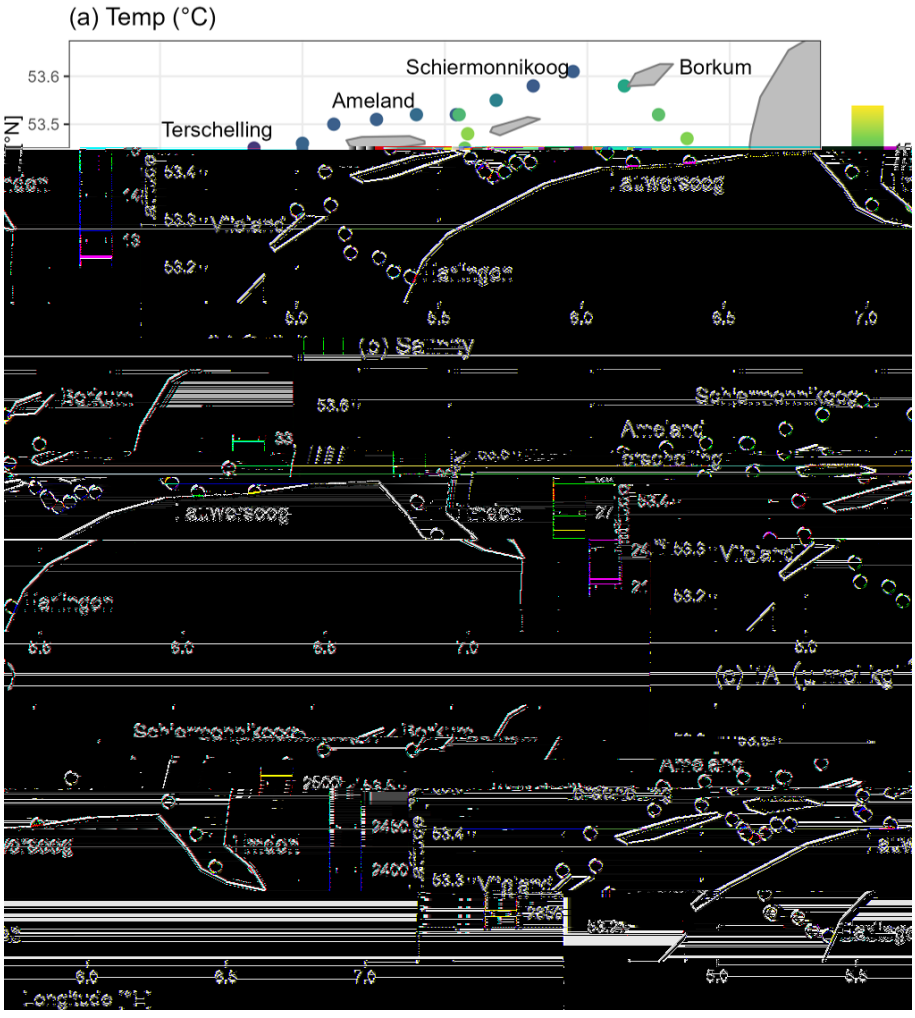

Figure 2. Spatial distribution of **(a)** temperature (°C), **(b)** salinity (PSU), and **(c)** total alkalinity (TA; $\mu mol\,kg^{-1}$) from surface water samples in May 2019.

imum values ($2273\,\mu mol\,DIC\,kg^{-1}$) at low tide, resulting in an increase of $101.3\,\mu mol\,DIC\,kg^{-1}$ (ΔDIC), or $14.9\,\mu mol\,DIC\,kg^{-1}\,h^{-1}$ (Fig. 4d). DIC increased almost twice as much as TA.

Nitrate increased by $0.92\,\mu mol\,NO_3{}^-\,L^{-1}$ ($\Delta NO_3{}^-$) during ebb tide, from a minimum of $1.26\,\mu mol\,NO_3{}^-\,L^{-1}$ to a maximum of $2.17\,\mu mol\,NO_3{}^-\,L^{-1}$ (Fig. 4e), resulting in a nitrate increase of $0.13\,\mu mol\,NO_3{}^-\,L^{-1}\,h^{-1}$.

Silicate showed a similar pattern, with low values ($1.8\,\mu mol\,Si\,L^{-1}$) at high tide that increased during ebb tide to a maximum of $11.2\,\mu mol\,Si\,L^{-1}$, resulting in a silicate increase (ΔSi) of $9.4\,\mu mol\,Si\,L^{-1}$, or $1.4\,\mu mol\,Si\,L^{-1}\,h^{-1}$, during ebb tide (Fig. 4f).

Ammonium increased from 3.47 to $6.22\,\mu mol\,NH_4{}^+\,L^{-1}$ during ebb tide (Fig. 4g), resulting in an ammonium increase ($\Delta NH_4{}^+$) of $2.74\,\mu mol\,NH_4{}^+\,L^{-1}$, or $0.4\,\mu mol\,NH_4{}^+\,L^{-1}\,h^{-1}$.

The calcite and aragonite saturation states had maximum values ($\Omega_{Ca} = 3.8$, $\Omega_{Ar} = 2.4$) at high tide and decreased to their minimum ($\Omega_{Ca} = 3.1$, $\Omega_{Ar} = 2.0$) during ebb tide (Fig. 4h). The influence of the North Sea is indicated by the observed maximum at high tide, which decreased during the ebb.

The seawater pCO_2 had minimum values at high tide (385.1 µatm) and increased up to 576.6 µatm during low tide (Fig. 4i).

Like Ω, the maximum pH was 8.07 at high tide and decreased to a minimum (7.93) during ebb tide (Fig. 4j).

The $C_{org} : N$ ratios of SPM increased during ebb tide (Fig. 4k). A minimum $C_{org} : N$ ratio of 5.6 was observed around high tide and increased to a maximum of 13.0 during ebb tide. Simultaneously, the SPM concentration increased during ebb tide, from $12.8\,mg\,SPM\,L^{-1}$ to a maximum of $82.4\,mg\,SPM\,L^{-1}$ at the second-last station (Table B1).

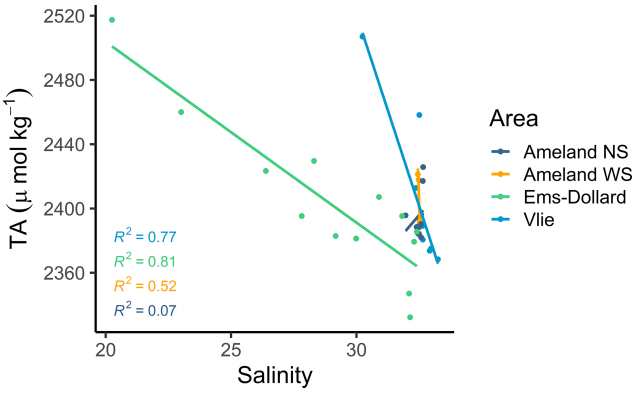

Figure 3. Mixing plot of total alkalinity (TA) and salinity (PSU) on the North Sea side of Ameland and the Frisian Inlet (Ameland NS), on the Wadden Sea side of Ameland (Ameland WS), around Schiermonnikoog and in the Ems-Dollard Inlet (Ems-Dollard), and in the Vlie Inlet (Vlie).

3.3 TA generation

Tidal forcing leads to an exchange between Wadden Sea and North Sea water almost twice a day. The tidal forcing also induces a strong benthic–pelagic coupling (Huettel et al., 2003; Røy et al., 2008). Many studies support the fact that outflowing water exports material from the sediment, including remineralization products from organic matter (e.g., Billerbeck et al., 2006; Røy et al., 2008). Here, we focus on the hypothesis that the sediments are a significant source of TA.

For an initial rough estimate of maximum TA export during ebb tide, we used the mean observed TA increase ($\Delta TA/2$) of 25.8 µmol TA kg^{-1} during ebb tide (in the Ameland Inlet, part of the Borndiep tidal basin), a tidal prism of 478×10^6 m^3 of the Borndiep tidal basin, and a share of intertidal flats of 53 % (Louters and Gerritsen, 1994). Assuming that only the intertidal sediments exchange TA, we estimated a TA export of 6.6 Mmol TA per tide to the North Sea. Assuming two ebb tides and a lunar cycle of 24.8 h, this would result in a daily export of 12.7 Mmol TA.

The significant correlation of TA and silicate ($R^2 = 0.93$) as well as the insignificant relation between TA and salinity ($R^2 = 0.32$) and between silicate and salinity ($R^2 = 0.21$) suggest that TA originates from the tidal flats in this part of the Dutch Wadden Sea, not from admixture carried by river runoff. The significant correlation between TA and silicate during ebb tide point to the same source (Fig. 5b).

To further elucidate potential TA sources in the Dutch Wadden Sea, we correlated TA with DIC, silicate, nitrate, and ammonium, respectively, in half a tidal cycle, from high tide to low tide (Fig. 5).

The correlation between TA and DIC is a measure between anaerobic and aerobic processes. Our data show a strong positive correlation between DIC and TA ($R^2 = 0.93$), with TA concentrations being higher than DIC concentrations (Fig. 5a). We observed a release of excess DIC compared with TA, as indicated by the slope of 1.89 and by an increase in DIC ($\Delta DIC = 101.3$ µmol kg^{-1}) that is almost twice as high as TA ($\Delta TA = 51.6$ µmol kg^{-1}) (Fig. 5a). This excess DIC may be caused by strong CO_2 production due to high aerobic OM degradation, which can be supported by the seawater pCO_2 being supersaturated with respect to the atmosphere (Fig. 4i). The TA increase can be fueled by various processes, which we will discuss below. We detected a positive linear correlation of increasing TA and silicate ($R^2 = 0.93$) during ebb tide, supporting pore water outflow (Fig. 5b), as pore water is the major Si source during summer (van Bennekom et al., 1974). A stronger influence of pore water with the ongoing ebb tide is indicated by increasing values. The positive correlation between nitrate and TA ($R^2 = 0.67$) (Fig. 5c) was less strong than the correlations between TA and DIC and between TA and Si, which could be traced back to an effect of the first four sampling points that were probably at the tipping point from high tide to low tide. In the remaining samples, the increasing nitrate and TA concentrations suggest stronger TA generation than nitrate production, balancing TA that may be consumed by nitrification (i.e., nitrate production).

4 Discussion

4.1 TA spatial variability

Hoppema (1990) reported TA distributions in the westernmost part of the Dutch Wadden Sea, around the barrier islands of Texel, Vlieland, and Terschelling. The aforementioned work focused on the tidal basins drained by the tidal inlets of Marsdiep and Vlie, located more to the west than our sampling stations (not visible on the map). Hoppema (1990) did not observe a continuous increase in salinity in the Wadden Sea from the freshwater source towards the North Sea and associated this with the influence of tidal differences and an arbitrary sampling scheme. The presence (dominance) of North Sea water in the Dutch Wadden Sea and on the tidal flats is supported by our transect data, which show relatively high salinities at the coastal North Sea level. Brackish salinity values were only detected in the Ems-Dollard Inlet, which receives freshwater from the river Ems, and close to Harlingen and Lauwersoog, which have direct freshwater inflows from smaller rivers and streams. The absence of clear salinity gradients in the more eastern part of the Dutch Wadden Sea investigated in our study suggests that most of the IJsselmeer discharge was exchanged with the North Sea through the Marsdiep Inlet (e.g., Duran-Matute et al., 2014).

The spatial TA data from Hoppema (1990) show lower TA concentrations at stations with more freshwater influence and higher TA concentrations in the tidal inlets. The data from this study also show high TA concentrations in the tidal inlets, suggesting TA generation in sediments, which

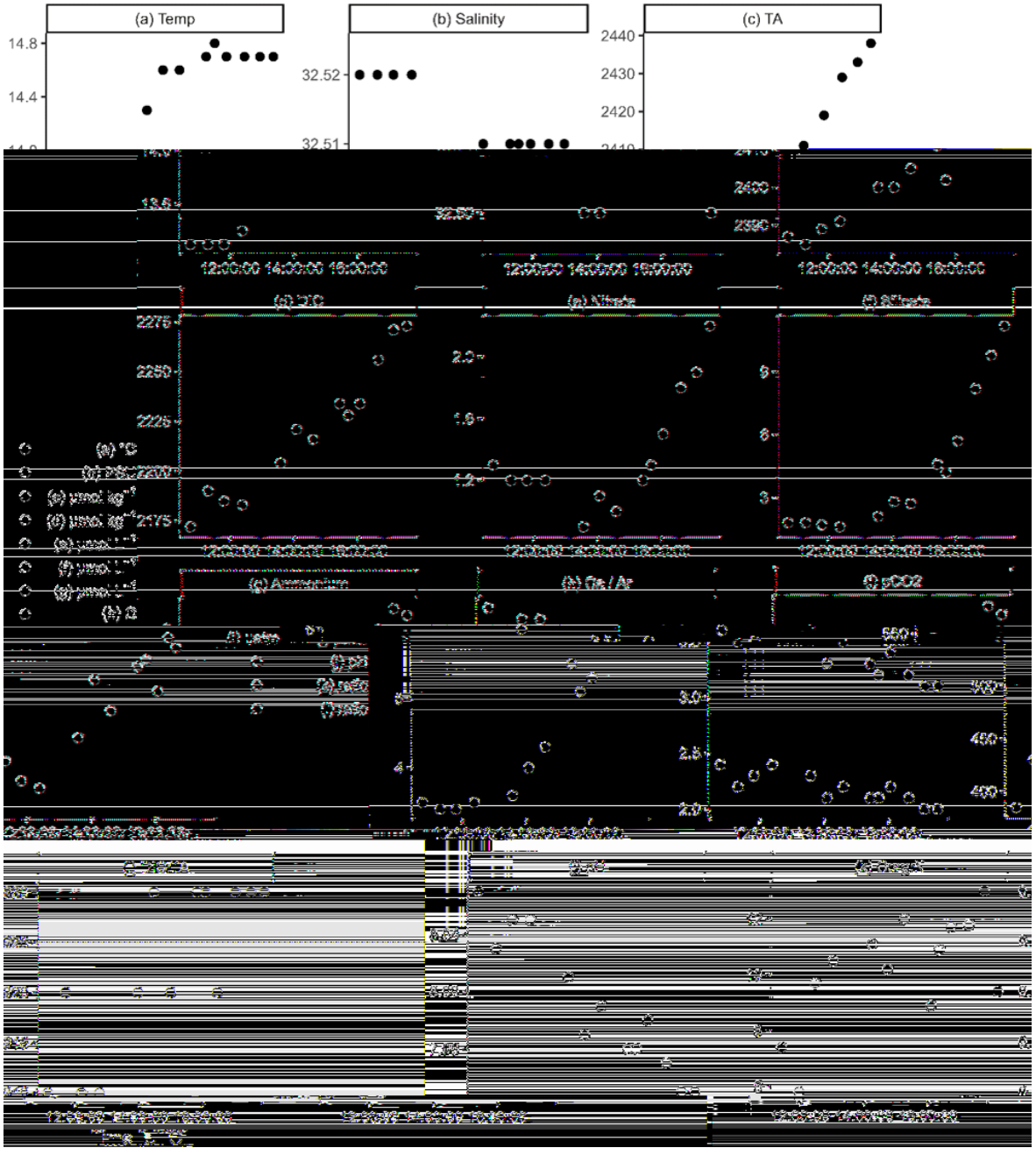

Figure 4. Half a tidal cycle (from high tide to low tide) showing the temporal distribution of **(a)** temperature, **(b)** salinity, **(c)** total alkalinity (TA), **(d)** dissolved inorganic carbon (DIC), **(e)** nitrate, **(f)** silicate, **(g)** ammonium, **(h)** calcite (upper points) and aragonite (lower points) saturation states, **(i)** pCO_2, **(j)** pH, **(k)** the C_{org} : N ratio of SPM, and **(l)** the DIC : TA ratio. Note the different y axes and the $+2$ h time difference between the local summer time and UTC time.

is possibly fueled by high nutrient and OM imports (van Beusekom and De Jonge, 2002). The even higher TA concentrations at stations with lower salinities close to the mainland observed in this study also show the influence of the catchment area on the coast and, possibly, TA generation in the shallow sediments near the coast. In May 1986, Hoppema (1990) found TA concentrations ranging between 2319 and 2444 µmol TA kg^{-1} at salinities between 18.62 and 29.17 PSU. Our lowest observed TA concentration was 2332 µmol TA kg^{-1} at a salinity of 32.14 PSU, whereas our highest TA concentration was 2517 µmol TA kg^{-1} at a salinity of 20.25 PSU close to the coastal mainland. A comparison of both studies shows that the general TA levels are in a similar range but that the spatial gradients are opposite.

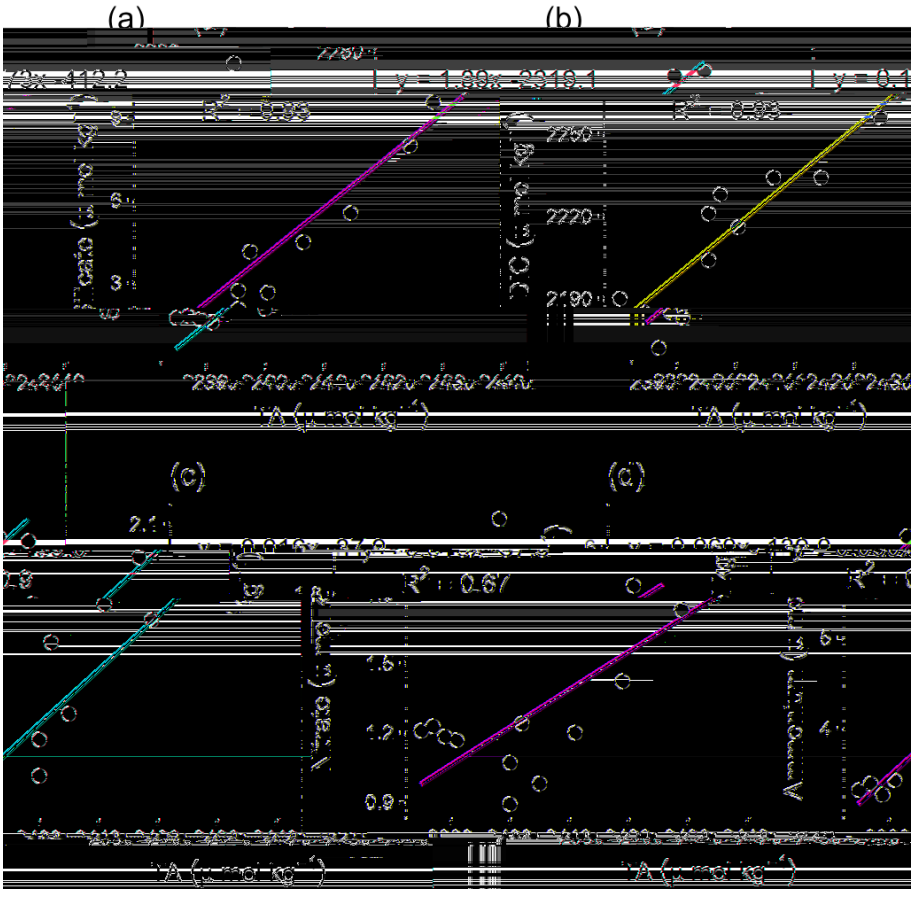

Figure 5. Correlations of TA with **(a)** dissolved inorganic carbon (DIC), **(b)** silicate, **(c)** nitrate, and **(d)** ammonium during ebb tide in the Ameland Inlet.

Conservative mixing between TA and salinity is only visible in the Ems-Dollard Inlet and the Vlie Inlet (Fig. 3). While conservative mixing in the Ems-Dollard Inlet is more dominated by the freshwater discharge from the river Ems, the conservative mixing in the Vlie Inlet is more dominated by North Sea water passing through this deep inlet and allowing more North Sea water to be transported towards the coast. After the Marsdiep Inlet, the Vlie Inlet has the highest average tidal prism and is the second-largest inlet in the Dutch Wadden Sea (Elias et al., 2012). Similar to our findings, Hoppema (1990) noted linear mixing of TA and salinity in the Vlie Inlet and also suspected a lower freshwater contribution in the inlet, which is in accordance with model data (Duran-Matute et al., 2014).

In the Ems-Dollard Inlet, conservative mixing was observed, indicating minor contributions from other sources. In a previous study, Norbisrath et al. (2023) observed very high TA concentrations and TA generation in the upper tidal river of the highly turbid Ems Estuary, which may explain the high levels of TA in the Ems-Dollard Inlet (at low salinities) observed in this study.

Hoppema (1990) also observed a range of TA concentrations in the Dutch Wadden Sea and related these to different sinks and sources. TA sinks can be calcium carbonate ($CaCO_3$) precipitation or the extraction of seawater carbonate by mollusks (e.g., Chen and Wang, 1999; Hoppema, 1990). Variable freshwater inflows can either serve as a sink or a source (e.g., Chen and Wang, 1999; Hoppema, 1990). Other TA sources can be $CaCO_3$ dissolution, anaerobic metabolic processes in the sediment, or the erosion of sediments that enhance TA (e.g., Hoppema, 1990; Chen and Wang, 1999).

Except for the Ems-Dollard Inlet and close to Harlingen, we mainly observed marine salinities > 30 PSU but found higher TA values in the Dutch Wadden Sea than in the North Sea. Therefore, we exclude possible TA sinks and focus only on TA sources. According to Hoppema (1990), the main causes of TA variation in the Dutch Wadden Sea were freshwater inflows and sources in the sediment. In our study, freshwater inflows with high TA concentrations were only observed in the Ems-Dollard Inlet (but not around the islands and the tidal flats). For a further TA source identification in

the Dutch Wadden Sea, we investigated the TA variability during ebb tide in a tidal channel close to Ameland.

4.2 Determination of TA generation

Burt et al. (2016) and Schwichtenberg et al. (2020) have indicated that TA generation in the Wadden Sea is an important source with respect to the North Sea's carbon storage capacity. Here, we want to further identify TA generation and potential TA sources.

In a study from the late 1980s, Hoppema (1993) observed a tidal cycle in the Marsdiep Inlet in May and September. Focusing on TA, DIC, and oxygen, this aforementioned work also observed increasing TA values during ebb tide and assumed that the tidal flats and discharging rivers and canals were TA sources. Comparing our present TA data to the historical TA data, there is not a large difference in the range of values observed during a tidal cycle. However, further in-depth interpretation and comparison of both TA data sets is limited by the low number of data, leading us to focus on TA generation during our cruise.

We made a very rough first estimate of the daily TA export. Using a 3D ecosystem model, Schwichtenberg et al. (2020) estimated an annual export of 10–14 $\mathrm{Gmol\,TA\,yr^{-1}}$ for the entire Dutch Wadden Sea. Given that the Borndiep tidal basin covers about 14 % of the Dutch Wadden Sea and assuming no seasonal dynamics, our estimate of 12.7 $\mathrm{Mmol\,TA\,d^{-1}}$ compares well with the annual average model estimate of 4.6 $\mathrm{Mmol\,TA\,d^{-1}}$, but the overestimation suggests that seasonal dynamics may be involved. As our TA export was based on only a half-tidal-cycle observation, the inclusion of it into the model used by Schwichtenberg et al. (2020) would be unreliable (Johannes Pätsch, personal communication, 2022). To test whether the observed TA generation matches their suggested TA export, observational data of at least each season are required to run the model and gain a representative result (Johannes Pätsch, personal communication, 2022).

4.3 TA source attribution

4.3.1 Local sediment outwash

In order to gain further insight into potential sources of TA, we compared our TA and nutrient data. The main focus was on dissolved silicate (Si), as van Bennekom et al. (1974) showed that this nutrient is depleted in the Wadden Sea during the spring diatom blooms and further reported that pore water is the main source of dissolved silicate during summer. It is important to note that winter concentrations in the Rhine (the main contributor to the IJsselmeer) have not changed much since the 1970s, showing maximum concentrations of about 125 $\mathrm{\mu mol\,Si\,L^{-1}}$ in winter and clear seasonal dynamics due to uptake by diatoms (unpublished results based on data provided by Pätsch, 2024: available from https://wiki.cen.uni-hamburg.de/ifm/ECOHAM/DATA_RIVER, last access: 30 July 2024). We identified a silicate increase of 1.4 $\mathrm{\mu mol\,Si\,L^{-1}\,h^{-1}}$ during ebb tide. Due to the absence of large estuaries nearby and salinity consistently being above 32 PSU at our tidal sampling station near the island of Ameland, we exclude freshwater runoff as a major silicate source and indicate TA sources within the Wadden Sea.

Submarine groundwater discharge (SGD) has been identified as a source for nutrient fluxes in tidal-flat ecosystems in previous studies (e.g., Billerbeck et al., 2006; Røy et al., 2008; Santos et al., 2021; Waska and Kim, 2011; Wu et al., 2013). As we observed relatively constant marine salinities, we suspect that deep pore water flow (e.g., Røy et al., 2008) which is enriched with respect to nutrients acts as a source for our observed increasing TA and nutrient parameters. TA generation in tidal flats was also observed by Faber et al. (2014), who focused on a large macro-tidal embayment in southern Australia. They also found increasing TA values during ebb tide, associated the TA increase with a higher fraction of pore water, and determined that the tidal cycle was the controlling force with respect to pore water exchange. Their findings and the observed silicate outwash support our assumption that TA is generated in the sediments of the tidal flats and is washed out during ebb tide. In addition, we exclude laterally advected signals from regions west of the Vlie Inlet, as the TA concentrations in the surface transect samples in the Vlie Inlet (except for the two samples close to the coastal mainland near Harlingen) were in the same range as the other observed TA concentrations and were lower than the increasing TA concentrations during ebb tide. Both increases in TA and silicate are tidal signals, and we identify TA generation in the sediments of the tidal flats here as the major local TA source.

4.3.2 TA generation processes

The observed TA increase of 7.6 $\mathrm{\mu mol\,TA\,kg^{-1}\,h^{-1}}$ and the silicate increase of 1.4 $\mathrm{\mu mol\,Si\,L^{-1}\,h^{-1}}$ indicated an excess of TA compared with silicate (also Fig. 5b). Considering a supposed TA : Si ratio of 2 : 1 (Marx et al., 2017), the observed 1.4 $\mathrm{\mu mol\,Si\,L^{-1}\,h^{-1}}$ would then account for a TA generation of 2.8 $\mathrm{\mu mol\,TA\,kg^{-1}\,h^{-1}}$. High silicate concentrations in tidal-flat pore water (Rutgers van der Loeff, 1974) and in situ production of silicate from dissolving diatom frustules are the most probable sources of the silicate (e.g., van Bennekom et al., 1974). As we observed more TA generated than silicate being washed out, other biogeochemical processes must be responsible for the TA generation in the sediments of the tidal flats in the Dutch Wadden Sea.

We exclude $CaCO_3$ dissolution as a TA source in the water column, as the Ω values were supersaturated with $\Omega > 1$ (Fig. 4h, Table B1). The continuous calcite supersaturation nicely indicated the inflow and dominance of North Sea water during the flood, with Ω values similar to previously observed North Sea values ($\Omega \sim 3.5$–4) (Charalampopoulou et

al., 2011; Carter et al., 2014). In pore water, carbonate undersaturation and associated $CaCO_3$ dissolution can only be driven metabolically, due to CO_2 production by OM remineralization or due to the reoxidation of compounds reduced previously by anaerobic processes (Brenner et al., 2016; Jahnke et al., 1994).

Other potential sources of TA generation in the sediments can be further narrowed down by a more detailed interpretation of changes in DIC (ΔDIC) and TA (ΔTA) during ebb tide as well as their combination with various nutrient ratios. The correlation of DIC and TA reveals an increase in DIC (ΔDIC) that is almost twice as high as that in TA (ΔTA) (Fig. 5a), as indicated by the slope of 1.89. The high ΔDIC points to high aerobic OM degradation and remineralization, resulting in high CO_2 production, which is also indicated by seawater being supersaturated with respect to pCO_2. High aerobic OM degradation has also previously been observed in the heterotrophic Wadden Sea (e.g., De Beer et al., 2005; van Beusekom et al., 1999), assuming OM degradation and remineralization occurring in the water and sediment in about equal parts (van Beusekom et al., 1999). High OM degradation is indicated by the increasing $C_{org} : N$ ratios of SPM during ebb tide (Fig. 4k, Table B1). Because we observed constant coastal North Sea salinities, we rule out freshwater runoff and terrestrial signals as a source of the increasing $C_{org} : N$ ratios of SPM. We assume that fresh OM is rapidly degraded in the water column and that the older OM settles on and in the sediment, where the degradation continues and where it is resuspended at low prevailing water levels during ebb. Therefore, we assume that the increase in the SPM concentrations and their $C_{org} : N$ ratios is an indicator of older and more refractory OM. The increase in TA concentrations points to anaerobic processes, $CaCO_3$ dissolution, or a combination thereof as TA sources occurring in the sediments.

For an upper-bound estimate of sedimentary $CaCO_3$ dissolution as source of TA, we considered a ΔDIC : ΔTA ratio of 1 : 2. Considering this ratio and the observed ΔTA of 51.6 µmol TA kg^{-1}, $CaCO_3$ dissolution would lead to a ΔDIC of 25.8 µmol DIC kg^{-1}. The remaining 75.5 µmol DIC kg^{-1} (101.3–25.8 µmol DIC kg^{-1}) of the observed ΔDIC in this study could then be produced by OM degradation and remineralization, and it would, using the theoretical expected Redfield ratio of C : N (6.6) for fresh OM (Hickel, 1984), correspond to an estimated dissolved inorganic nitrogen (DIN) production of 11.4 µmol DIN kg^{-1}. However, this estimated DIN production (11.4 µmol DIN kg^{-1}) of OM degradation and remineralization exceeds the observed increase in ΔDIN (3.97 µmol DIN L^{-1}, sum of NO_3^-, NO_2^- and NH_4^+; Table B1) during ebb tide. Based on this estimation and the assumption that all DIN produced is released and, thus, lost, TA is probably produced by $CaCO_3$ dissolution and anaerobic metabolic processes other than denitrification in the sediment. In addition to that, and with an N-focused perspective, the DIN loss also hints at the occurrence of other processes that consume nitrogen species but have no net effect on TA, such as anammox and coupled nitrification–denitrification (Hu and Cai, 2011; Middelburg et al., 2020). The suggested DIN loss can be supported by considering the marine DIN : Si ratio, which is supposed to be about 1 : 1 (Brzezinski, 1985). We observed DIN : Si ratios decreasing from 2.7 to 0.8 during ebb tide, showing that both parameter concentrations increased, whereby DIN concentrations increased less than silicate concentrations. The silicate excess with respect to DIN at the end of ebb tide supports the DIN loss.

Denitrification, the anaerobic irreversible reduction of NO_3^- to N_2 that generates 0.9 mol of TA using 1 mol of NO_3^- as an electron acceptor (Chen and Wang, 1999), is a net TA source. Denitrification depends on the supply of nitrate, which seasonally varies (van der Zee and Chou, 2005, and references therein). Generally, nitrate is depleted in summer due to high photosynthetic activity and occurs in higher concentrations in winter (Kieskamp et al., 1991; Jensen et al., 1996; van der Zee and Chou, 2005). This seasonality leads to denitrification rates also being lower in summer and higher in winter (Kieskamp et al., 1991; Jensen et al., 1996). In previous studies, Faber et al. (2014) identified denitrification as a minor source of TA due to low denitrification rates, and Kieskamp et al. (1991) also observed low denitrification rates in the Wadden Sea, with low nitrate concentrations (< 2.5 µmol NO_3^- L^{-1}) in the water column. We observed nitrate concentrations (< 2.17 µmol NO_3^- L^{-1}) lower than the concentration sufficient for denitrification assumed by Kieskamp et al. (1991). Therefore, we do not exclude denitrification; rather, we suspect it as a minor source of TA in the Dutch Wadden Sea, at least in spring and summer, due to the seasonal lack of nitrate. Thomas et al. (2009) detected TA seasonality in the southern bight of the North Sea, which is also influenced by the TA generation in the Wadden Sea. In addition, the estimated DIN production compared to the observed DIN not only hints at other N-consuming processes that have no effect on TA but also suggests that allochthonous nitrate would be needed to fuel the TA increase by denitrification.

The simultaneous increase in ammonium and TA (Figs. 4c and d and 5d) is important to notice, because the occurrence of ammonium is coupled with nitrification, a process that consumes ammonium and also TA, under oxic conditions (Chen and Wang, 1999). However, under anoxic conditions, such as in deeper sediment layers, ammonium cannot be reoxidized, accumulates, and is washed out during ebb tide. As we observed low nitrate concentrations and rule out terrestrial nitrate inputs here, the increase in ammonium and TA implies the occurrence of other anaerobic processes of the redox system, such as sulfate and iron reduction, to generate TA in the deeper, anoxic sediment layers in the Dutch Wadden Sea.

Sulfate reduction followed by iron reduction and the formation and burial of pyrite are net sources of TA, as TA

consumption by reoxidation is excluded when buried in sediments (Berner et al., 1970; Faber et al., 2014). Whether and to what extent these processes contribute to TA generation in the deeper sediments of the Dutch Wadden Sea cannot be further identified without the necessary data. However, sulfate reduction was also mentioned as source of TA by Thomas et al. (2009), and the temporary slight appearance of a noticeable sulfuric odor could be another indirect indicator of the occurrence of sulfate reduction. In previous studies of tidal flats in the German Wadden Sea, Beck et al. (2008a, b) observed increasing TA concentrations with depth and identified sulfate reduction as the most important process for anaerobic OM remineralization in pore water cores.

A strict comparison of the more northern (north of the Elbe Estuary) and the more western (Texel – Elbe Estuary) parts of the Wadden Sea is difficult, as the areas vary in terms of OM import and eutrophication effects (van Beusekom et al., 2019), sediment composition, and the distance between the barrier islands and the mainland, all of which influence the occurrence and interaction of biogeochemical processes (Schwichtenberg et al., 2020). The area characteristics of the northern and western Wadden Sea specifically differ in terms of the OM turnover being lower in the more northern Wadden Sea. However, a previous study by Brasse et al. (1999) identified high TA and DIC concentrations in the sediment of the North Frisian Wadden Sea and identified $CaCO_3$ dissolution and sulfate reduction as major TA sources, which is consistent with our findings.

5 Conclusion

The Dutch Wadden Sea is a unique and highly dynamic ecosystem. We observed higher TA values in the Dutch Wadden Sea than in the North Sea and identified the Dutch Wadden Sea as a TA source for the North Sea's carbonate system. Compared to previous studies (Hoppema, 1990, 1993), the TA values that we observed were in a similar range, with high TA values in the tidal basins. In addition to the need for seasonal observations, future work should also focus on the regional and seasonal impacts of freshwater inflows of TA on the TA status in the Dutch Wadden Sea.

By observing salinity and using dissolved silicate as a tracer, we excluded freshwater and river runoff as significant TA sources on the tidal flats and, instead, deduced local outwash from the sediments as sources of TA. Considering various stoichiometries, we suggest that $CaCO_3$ dissolution generates TA in the more upper, oxic sediment layers and that anaerobic metabolic processes such as denitrification, sulfate, and iron reduction are potential TA sources in the deeper, anoxic sediment layers. However, in spring and early summer, denitrification seems to play a minor role in generating TA in the sediments of the Dutch Wadden Sea due to seasonality and associated limited nitrate availability.

Appendix A

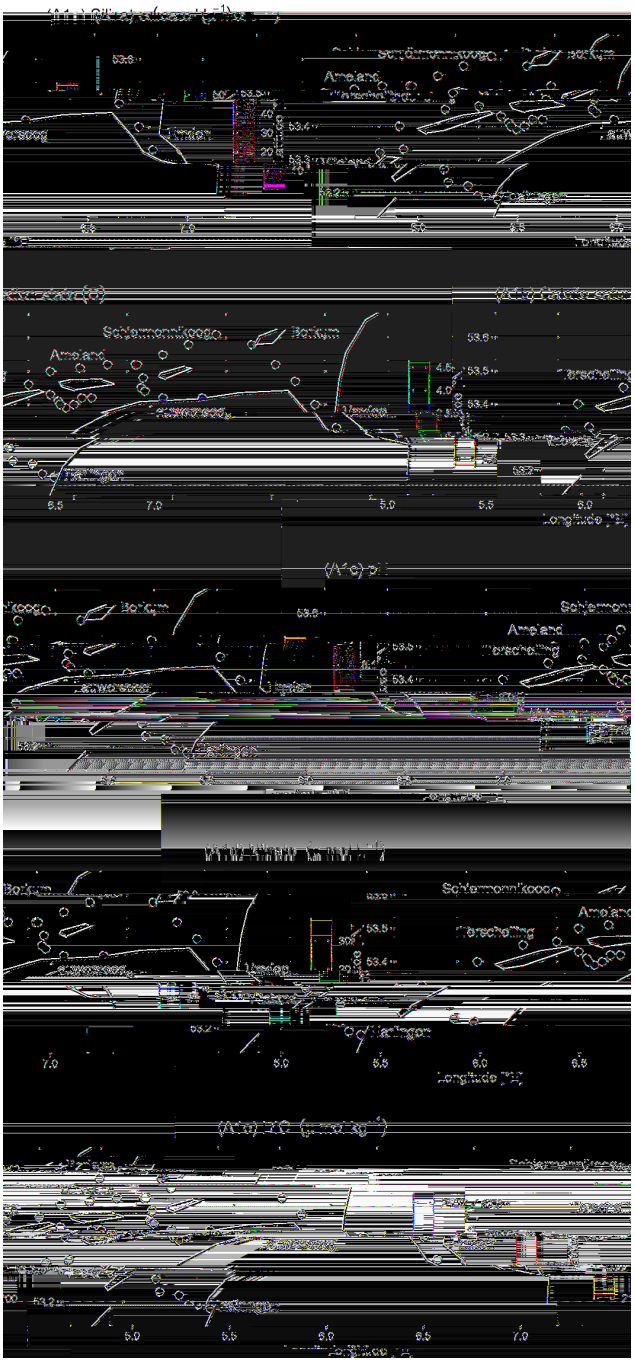

Figure A1. Spatial distribution of **(a)** silicate (Si; $\mu mol\,L^{-1}$), **(b)** calcite saturation state (Ω), **(c)** pH, **(d)** nitrate (NO_3^-; $\mu mol\,L^{-1}$), and **(e)** dissolved inorganic carbon (DIC; $\mu mol\,kg^{-1}$) from surface water samples in May 2019.

Appendix B

Table B1. Half-tidal-cycle sample parameters during ebb tide. Sample no. 545 is the first sample at high tide and sample no. 557 is the last sample at low tide on 21 May 2019 (53.38° N and 5.62° E). Shown are values of temperature (Temp), salinity (Sal), total alkalinity (TA), dissolved inorganic carbon (DIC), silicate (Si), nitrate (NO_3^-), nitrite (NO_2^-), ammonium (NH_4^+), phosphate (PO_4^{3-}), dissolved inorganic nitrogen (DIN), the amount of carbon (C) and organic carbon (C_{org}) in SPM, the amount of nitrogen (N) in SPM, the calcite (Ca) and aragonite (Ar) saturation states, the pH, and the seawater partial pressure of CO_2 (pCO_2) per sample.

Sample no.	Time (UTC)	Temp (°C)	Sal (PSU)	TA / DIC ($\mu mol\,kg^{-1}$)	Si ($\mu mol\,L^{-1}$)	NO_3^- ($\mu mol\,L^{-1}$)	NO_2^- ($\mu mol\,L^{-1}$)	NH_4^+ ($\mu mol\,L^{-1}$)	PO_4^{3-} ($\mu mol\,L^{-1}$)
545	10:46	13.26	32.52	2387 / 2172	1.84	1.26	0.19	3.47	0.12
546	11:19	13.25	32.52	2385 / 2190	1.77	1.24	0.19	3.40	0.11
547	11:49	13.28	32.52	2389 / 2185	1.72	1.21	0.19	3.35	0.11
548	12:23	13.38	32.52	2391 / 2183	1.6	1.19	0.19	3.52	0.12
549	13:35	14.32	32.50	2400 / 2204	2.11	0.91	0.25	3.57	0.32
550	14:05	14.61	32.50	2400 / 2221	2.78	1.09	0.29	3.98	0.42
551	14:36	14.64	32.51	2405 / 2216	2.72	1.01	0.29	4.27	0.47
552	15:26	14.73	32.51	2411 / 2234	4.59	1.23	0.34	5.51	0.57
553	15:42	14.77	32.51	2402 / 2228	4.24	1.26	0.33	5.08	0.54
554	16:04	14.72	32.51	2419 / 2234	5.66	1.46	0.36	5.33	0.54
555	16:38	14.66	32.51	2428 / 2256	8.18	1.77	0.43	6.04	0.58
556	17:07	14.68	32.51	2433 / 2271	9.79	1.87	0.47	6.27	0.62
557	17:32	14.70	32.50	2438 / 2273	11.22	2.17	0.50	6.22	0.63

Sample no.	Time (UTC)	DIN ($\mu mol\,L^{-1}$)	C / C_{org} (SPM) ($\mu mol\,L^{-1}$)	N (SPM) ($\mu mol\,L^{-1}$)	C_{org} : N (SPM)	SPM ($mg\,L^{-1}$)	Ca / Ar (Ω)	pH	pCO_2 (µatm)
545	10:46	4.93	86.8 / 65.1	8.8	7.4	12.8	3.8 / 2.4	8.07	385.1
546	11:19	4.83	72.7 / 42.4	7.4	5.8	8.7	3.5 / 2.3	8.03	430.2
547	11:49	4.76	112.4 / 93.4	9.6	9.7	15.4	3.7 / 2.3	8.05	411.4
548	12:23	4.91	108.5 / 104.6	9.9	10.5	16.8	3.7 / 2.4	8.05	404.1
549	13:35	4.73	111.1 / 97.8	8.8	11.1	13.9	3.6 / 2.3	8.01	452.3
550	14:05	5.37	233.0 / 180.3	17.7	10.2	32.2	3.3 / 2.1	7.97	507.2
551	14:36	5.56	193.2 / 174.3	14.5	12.0	29.6	3.5 / 2.2	7.99	477.9
552	15:26	7.08	248.6 / 163.5	18.4	8.9	34.3	3.3 / 2.1	7.96	520.0
553	15:42	6.67	257.6 / 199.3	18.3	10.9	41.6	3.2 / 2.1	7.95	526.4
554	16:04	7.15	324.4 / 271.1	23.2	11.7	55.0	3.4 / 2.2	7.98	496.6
555	16:38	8.24	440.4 / 345.2	29.2	11.8	75.7	3.2 / 2.1	7.95	538.0
556	17:07	8.61	430.5 / 363.3	27.9	13.0	82.4	3.1/ 2.0	7.93.	576.6
557	17:32	8.90	308.9 / 199.1	21.2	9.4	48.8	3.1 / 2.0	7.93	568.4

Table B2. Half-tidal-cycle sample parameters during high tide for comparison. Sample no. 564 is the first sample at low tide and sample no. 578 is the last sample at high tide on 23 May 2019 (53.39° N and 5.63° E, 5.62° E*). Shown are values of temperature (Temp), salinity (Sal), total alkalinity (TA), dissolved inorganic carbon (DIC), silicate (Si), nitrate (NO_3^-), nitrite (NO_2^-), ammonium (NH_4^+), phosphate (PO_4^{3-}), dissolved inorganic nitrogen (DIN), the amount of carbon (C) and organic carbon (C_{org}) in SPM, the amount of nitrogen (N) in SPM, the calcite (Ca) and aragonite (Ar) saturation states, the pH, and the seawater partial pressure of CO_2 (pCO_2) per sample.

Sample no.	Time (UTC)	Temp (°C)	Sal (PSU)	TA / DIC ($\mu mol\,kg^{-1}$)	Si ($\mu mol\,L^{-1}$)	NO_3^- ($\mu mol\,L^{-1}$)	NO_2^- ($\mu mol\,L^{-1}$)	NH_4^+ ($\mu mol\,L^{-1}$)	PO_4^{3-} ($\mu mol\,L^{-1}$)
564	05:09	14.04	32.66	2431 / 2246	8.53	1.25	0.47	3.31	0.38
565	05:32	14.02	32.68	2441 / 2287	9.14	1.26	0.45	3.08	0.37
566	06:01	13.95	32.69	2436 / 2284	8.88	1.33	0.38	2.46	0.34
567	06:33	14.16	32.69	2443 / 2284	8.68	0.95	0.37	2.37	0.33
568	07:02	14.21	32.69	2432 / 2280	6.94	0.75	0.34	2.63	0.32
569	07:31	14.15	32.55	2401 / 2223	2.12	0.98	0.27	4.12	0.33
570	08:04	14.20	32.55	2403 / 2218	2.10	1.04	0.27	3.88	0.30
571	08:35	14.27	32.55	2409 / 2228	2.15	0.92	0.25	4.18	0.32
572	09:04	14.37	32.53	2400 / 2209	1.88	1.00	0.22	3.86	0.26
573	09:34	14.16	32.52	2398 / 2200	1.70	1.03	0.21	3.51	0.21
574*	10:02	14.17	32.52	2391 / 2197	1.72	1.07	0.21	3.40	0.18
575*	10:34	14.11	32.51	2389 / 2195	1.78	1.18	0.20	3.45	0.16
576	11:04	14.21	32.50	2390 / 2187	1.76	1.12	0.19	3.29	0.14
577	11:34	14.50	32.51	2399 / 2193	1.66	1.10	0.20	3.32	0.16
578	12:03	13.96	32.51	2390 / 2187	1.75	1.41	0.19	3.72	0.11

Sample no.	Time (UTC)	DIN ($\mu mol\,L^{-1}$)	C / C_{org} (SPM) ($\mu mol\,L^{-1}$)	N (SPM) ($\mu mol\,L^{-1}$)	C_{org} : N (SPM)	SPM ($mg\,L^{-1}$)	Ca / Ar (Ω)	pH	pCO_2 (µatm)
564	05:09	5.03	353.7 / 253.2	27.5	9.2	52.3	3.0 / 2.2	7.99	490.3
565	05:32	4.78	333.5 / 220.1	26.1	8.4	49.7	3.0 / 1.9	7.92	592.9
566	06:01	4.17	330.3 / 232.9	25.5	9.1	51.7	2.9 / 1.9	7.91	600.3
567	06:33	3.68	274.7 / 195.7	21.8	9.0	36.9	3.0 / 1.9	7.92	582.6
568	07:02	3.72	317.8 / 220.2	24.5	9.0	46.1	2.9 / 1.9	7.91	601.8
569	07:31	5.37	88.6 / 59.1	7.0	8.5	14.7	3.3 / 2.1	7.98	500.7
570	08:04	5.20	96.8 / 73.6	8.8	8.4	18.1	3.4 / 2.2	7.99	482.6
571	08:35	5.35	114.2 / 109.6	9.9	11.0	14.8	3.3 / 2.1	7.98	497.6
572	09:04	5.08	107.5 / 73.9	9.9	7.5	16.4	3.5 / 2.2	8.00	466.6
573	09:34	4.75	82.1 / 72.7	7.2	10.0	11.8	3.6 / 2.3	8.02	445.3
574*	10:02	4.68	85.2 / 62.9	7.2	8.7	9.9	3.5 / 2.3	8.01	450.5
575*	10:34	4.83	83.5 / 65.9	7.2	9.2	11.1	3.5 / 2.3	8.01	449.6
576	11:04	4.60	82.7 / 52.1	8.2	6.3	8.5	3.7 / 2.3	8.03	429.9
577	11:34	4.62	65.8 / 50.8	6.5	7.8	7.2	3.7 / 2.4	8.03	430.8
578	12:03	5.32	71.6 / 54.6	7.7	7.1	7.7	3.7 / 2.3	8.04	425.3

Table B3. Transect parameters of cruise LP20190515 on RV *Ludwig Prandtl* in the Dutch Wadden Sea in May 2019. Shown are values of latitude (Lat), longitude (Long), temperature (Temp), salinity (Sal), total alkalinity (TA), dissolved inorganic carbon (DIC), silicate (Si), nitrate (NO_3^-), the calcite (Ca) and aragonite (Ar) saturation states, and pH per sample. Our salinity and temperature data were complemented by data from three Rijkswaterstaat stations, which were close to our stations. Of these three stations, Dantziggat[a] (53°24′4.093″ N, 5°43′37.132″ E) showed temperatures of 11.4 and 14.9 °C and salinities of 31.9 and 31.2 PSU on 10 and 27 May 2019, respectively; Terschelling 10[b] (53°27′37.318″ N, 5°5′58.129″ E) showed temperatures of 11.4 and 12.9 °C and salinities of 32.8 and 33.4 PSU on 15 and 28 May 2019, respectively; and Vliestroom[c] (53°18′48.054″ N, 5°9′35.655″ E) showed a temperature of 11.8 °C and a salinity of 31.1 PSU on 14 May 2019.

Sample no.	Time (UTC)	Day in May	Lat (° N)	Long (° E)	Temp (°C)	Sal (PSU)	TA / DIC ($\mu mol\,kg^{-1}$)	Si / NO_3^- ($\mu mol\,L^{-1}$)	Ca / Ar (Ω)	pH
535	07:56	20	53.18	5.4	14.72	30.24	2507 / 2357	10.00 / 5.10	3.0 / 1.9	7.92
536	08:26	20	53.19	5.34	14.81	32.51	2458 / 2296	3.45 / 0.46	3.1 / 2.0	7.92
537	08:53	20	53.22	5.29	14.05	32.38	2413 / 2227	1.92 / 0.85	3.4 / 2.2	8.00
538	09:28	20	53.23	5.19	13.36	32.65	2381 / 2153	0.52 / 1.02	4.0 / 2.6	8.10
539	09:53	20	53.27	5.17	13.17	32.65	2389 / 2161	0.45 / 1.37	4.0 / 2.6	8.10
540[c]	10:36	20	53.33	5.12	12.77	32.97	2375 / 2118	0.32 / 0.84	4.4 / 2.8	8.16
541	11:03	20	53.32	5.0	12.41	33.25	2368 / 2097	0.34 / 0.77	4.6 / 3.0	8.19
542[b]	11:49	20	53.4	5.1	12.93	32.92	2374 / 2109	0.44 / 0.81	4.6 / 2.9	8.17
543	12:49	20	53.45	5.33	12.95	32.45	2385 / 2196	6.25 / 1.85	3.4 / 2.2	8.02
544	13:31	20	53.46	5.5	13.55	32.51	2388 / 2169	3.02 / 1.30	3.9 / 2.5	8.08
558	11:33	22	53.41	5.65	13.31	32.51	2384 / 2224	2.57 / 1.56	3.0 / 1.9	7.95
559	12:04	22	53.4	5.66	13.45	32.51	2393 / 2195	1.58 / 1.41	3.6 / 2.3	8.03
560	12:40	22	53.39	5.69	13.67	32.52	2391 / 2183	1.52 / 1.33	3.7 / 2.4	8.05
561	13:09	22	53.4	5.73	14.23	32.48	2418 / 2242	2.04 / 1.04	3.3 / 2.1	7.97
562	13:32	22	53.42	5.77	14.71	32.51	2417 / 2237	3.23 / 1.04	3.3 / 2.1	7.97
563[a]	13:56	22	53.42	5.82	15.33	32.45	2421 / 2242	4.68 / 0.86	3.3 / 2.1	7.96
579	09:05	24	53.42	5.77	15.26	32.65	2417 / 2215	2.71 / 0.86	3.7 / 2.4	8.01
580	09:31	24	53.4	5.73	14.99	32.66	2426 / 2249	3.52 / 1.46	3.3 / 2.1	7.95
581	10:01	24	53.4	5.66	13.87	32.58	2396 / 2205	1.69 / 1.60	3.5 / 2.2	8.01
582	10:25	24	53.43	5.61	14.36	32.51	2389 / 2193	2.23 / 2.52	3.6 / 2.3	8.02
583	10:59	24	53.5	5.61	13.48	32.58	2382 / 2187	3.69 / 3.41	3.5 / 2.2	8.03
584	11:31	24	53.51	5.76	13.50	32.59	2390 / 2172	1.93 / 2.96	3.9 / 2.5	8.07
585	12:00	24	53.52	5.9	13.65	32.59	2390 / 2173	2.34 / 2.23	3.9 / 2.5	8.07
586	12:30	24	53.52	6.04	13.50	32.48	2384 / 2179	2.00 / 1.53	3.7 / 2.3	8.05
587	13:02	24	53.45	6.07	15.13	32.40	2389 / 2169	0.70 / 1.19	3.9 / 2.5	8.05
588	13:31	24	53.42	6.38	15.63	31.96	2396 / 2182	1.33 / 0.62	3.9 / 2.5	8.04
589	07:20	25	53.42	6.18	15.73	28.31	2430 / 2245	4.16 / 5.13	3.6 / 2.3	8.02
590	07:52	25	53.44	6.09	15.80	30.90	2407 / 2225	1.58 / 1.39	3.4 / 2.2	7.98
591	08:21	25	53.48	6.08	15.34	31.82	2395 / 2222	4.16 / 5.09	3.3 / 2.1	7.96
592	08:51	25	53.52	6.05	14.80	32.41	2386 / 2178	0.71 / 0.67	3.8 / 2.4	8.04
593	09:22	25	53.55	6.18	13.96	32.30	2379 / 2175	0.36 / 1.52	3.7 / 2.3	8.04
594	09:53	25	53.58	6.31	13.43	32.14	2332 / 2148	0.34 / 5.75	3.3 / 2.1	8.01
595	10:24	25	53.61	6.45	13.47	32.10	2347 / 2113	0.26 / 5.19	4.1 / 2.6	8.12
596	11:05	25	53.58	6.63	14.50	29.99	2381 / 2184	0.78 / 20.25	3.7 / 2.3	8.05
597	11:33	25	53.52	6.75	14.94	29.17	2383 / 2214	3.04 / 27.84	3.3 / 2.1	7.99
598	12:00	25	53.47	6.85	15.28	27.82	2395 / 2249	8.90 / 37.93	3.0 / 1.9	7.94
599	12:30	25	53.4	6.95	15.46	26.39	2423 / 2284	17.63 / 36.54	2.9 / 1.8	7.94
600	12:59	25	53.33	7.02	15.76	23.01	2460 / 2343	41.93 / 37.68	2.7 / 1.7	7.92
601	13:29	25	53.33	7.16	15.96	20.25	2517 / 2430	56.32 / 37.94	2.3 / 1.4	7.86

Data availability. The data generated and presented in this study are given in Appendix A and B.

Author contributions. MN wrote the manuscript, carried out the carbon sampling and sample measurement, analyzed and evaluated the data, and led the study. JEEvB led the research cruise. JEEvB and HT provided editorial and scientific recommendations. MN prepared the manuscript with contributions from all co-authors.

Competing interests. The contact author has declared that none of the authors has any competing interests.

Disclaimer. Publisher's note: Copernicus Publications remains neutral with regard to jurisdictional claims made in the text, published maps, institutional affiliations, or any other geographical representation in this paper. While Copernicus Publications makes every effort to include appropriate place names, the final responsibility lies with the authors.

Acknowledgement. The authors wish to thank the crew of the RV *Ludwig Prandtl* for their support during the cruise. We are also grateful to Leon Schmidt for the nutrient sampling and measurements, Marc Metzke for the C and N measurements, and Yoana Voynova and her department for the FerryBox preparation. We further thank the editor and two anonymous reviewers for their constructive comments, which greatly improved this paper.

Financial support. This research has been supported by the German Academic Exchange Service (DAAD; grant no. 57429828), which received funds from the German Federal Ministry of Education and Research (BMBF).

The article processing charges for this open-access publication were covered by the Helmholtz-Zentrum Hereon.

Review statement. This paper was edited by Mario Hoppema and reviewed by two anonymous referees.

References

Abril, G. and Frankignoulle, M.: Nitrogen–alkalinity interactions in the highly polluted Scheldt basin (Belgium), Water Res., 35, 844–850, https://doi.org/10.1016/S0043-1354(00)00310-9, 2001.

Beck, M., Dellwig, O., Holstein, J. M., Grunwald, M., Liebezeit, G., Schnetger, B., and Brumsack, H.-J.: Sulphate, dissolved organic carbon, nutrients and terminal metabolic products in deep pore waters of an intertidal flat, Biogeochemistry, 89, 221–238, https://doi.org/10.1007/s10533-008-9215-6, 2008a.

Beck, M., Dellwig, O., Liebezeit, G., Schnetger, B., and Brumsack, H.-J.: Spatial and seasonal variations of sulphate, dissolved organic carbon, and nutrients in deep pore waters of intertidal flat sediments, Estuar. Coast. Shelf S., 79, 307–316, https://doi.org/10.1016/j.ecss.2008.04.007, 2008b.

Berner, R. A., Scott, M. R., and Thomlinson, C.: Carbonate alkalinity in the pore waters of anoxic marine sediments, Limnol. Oceanogr., 15, 544–549, https://doi.org/10.4319/lo.1970.15.4.0544, 1970.

Berner, R. A., Lasaga, A. C., and Garrels, R. M.: Carbonate-silicate geochemical cycle and its effect on atmospheric carbon dioxide over the past 100 million years, Am. J. Sci., 283, 641–683, https://doi.org/10.2475/ajs.283.7.641, 1983.

Billerbeck, M., Werner, U., Polerecky, L., Walpersdorf, E., DeBeer, D., and Huettel, M.: Surficial and deep pore water circulation governs spatial and temporal scales of nutrient recycling in intertidal sand flat sediment, Mar. Ecol. Prog. Ser., 326, 61–76, 2006.

Borges, A. V., Delille, B., and Frankignoulle, M.: Budgeting sinks and sources of CO_2 in the coastal ocean: Diversity of ecosystems counts, Geophys. Res. Lett., 32, L14601, https://doi.org/10.1029/2005GL023053, 2005.

Bozec, Y., Thomas, H., Elkalay, K., and de Baar, H. J.: The continental shelf pump for CO_2 in the North Sea – evidence from summer observation, Mar. Chem., 93, 131–147, https://doi.org/10.1016/j.marchem.2004.07.006, 2005.

Brasse, S., Reimer, A., Seifert, R., and Michaelis, W.: The influence of intertidal mudflats on the dissolved inorganic carbon and total alkalinity distribution in the German Bight, southeastern North Sea, J. Sea Res., 42, 93–103, 1999.

Brenner, H., Braeckman, U., Le Guitton, M., and Meysman, F. J. R.: The impact of sedimentary alkalinity release on the water column CO_2 system in the North Sea, Biogeosciences, 13, 841–863, https://doi.org/10.5194/bg-13-841-2016, 2016.

Brewer, P. G. and Goldman, J. C.: Alkalinity changes generated by phytoplankton growth, Limnol. Oceanogr., 21, 108–117, https://doi.org/10.4319/lo.1976.21.1.0108, 1976.

Brzezinski, M. A.: The Si : C : N ratio of marine diatoms: interspecific variability and the effect of some environmental variables, J. Phycol., 21, 347–357, https://doi.org/10.1111/j.0022-3646.1985.00347.x, 1985.

Burchard, H., Flöser, G., Staneva, J. V., Badewien, T. H., and Riethmüller, R.: Impact of density gradients on net sediment transport into the Wadden Sea, J. Phys. Oceanogr., 38, 566–587, 2008.

Burt, W., Thomas, H., Hagens, M., Pätsch, J., Clargo, N., Salt, L., Winde, V., and Böttcher, M.: Carbon sources in the North Sea evaluated by means of radium and stable carbon isotope tracers, Limnol. Oceanogr., 61, 666–683, https://doi.org/10.1002/lno.10243, 2016.

Carter, B. R., Toggweiler, J. R., Key, R. M., and Sarmiento, J. L.: Processes determining the marine alkalinity and calcium carbonate saturation state distributions, Biogeosciences, 11, 7349–7362, https://doi.org/10.5194/bg-11-7349-2014, 2014.

Charalampopoulou, A., Poulton, A. J., Tyrrell, T., and Lucas, M. I.: Irradiance and pH affect coccolithophore community composition on a transect between the North Sea and the Arctic Ocean, Mar. Ecol. Prog. Ser., 431, 25–43, https://doi.org/10.3354/meps09140, 2011.

Chen, C. T. A. and Wang, S. L.: Carbon, alkalinity and nutrient budgets on the East China Sea continental shelf, J. Geophys. Res.-Oceans, 104, 20675–20686, https://doi.org/10.1029/1999JC900055, 1999.

Crutzen, P.: Geology of mankind, Nature, 415, 23, https://doi.org/10.1038/415023a, 2002.

De Beer, D., Wenzhöfer, F., Ferdelman, T. G., Boehme, S. E., Huettel, M., van Beusekom, J. E., Böttcher, M. E., Musat, N., and Dubilier, N.: Transport and mineralization rates in North Sea sandy intertidal sediments, Sylt-Rømø basin, Wadden Sea, Limnol. Oceanogr., 50, 113–127, 2005.

De Jonge, V., Essink, K., and Boddeke, R.: The Dutch Wadden Sea: a changed ecosystem, Hydrobiologia, 265, 45–71, https://doi.org/10.1007/BF00007262, 1993.

Dickson, A. and Millero, F. J.: A comparison of the equilibrium constants for the dissociation of carbonic acid in seawater media, Deep-Sea Res., 34, 1733–1743, https://doi.org/10.1016/0198-0149(87)90021-5, 1987.

Dickson, A. G.: An exact definition of total alkalinity and a procedure for the estimation of alkalinity and total inorganic carbon from titration data, Deep-Sea Res., 28, 609–623, https://doi.org/10.1016/0198-0149(81)90121-7, 1981.

Duran-Matute, M., Gerkema, T., de Boer, G. J., Nauw, J. J., and Gräwe, U.: Residual circulation and freshwater transport in the Dutch Wadden Sea: a numerical modelling study, Ocean Sci., 10, 611–632, https://doi.org/10.5194/os-10-611-2014, 2014.

Elias, E. P., Van der Spek, A. J., Wang, Z. B., and De Ronde, J.: Morphodynamic development and sediment budget of the Dutch Wadden Sea over the last century, Neth. J. Geosci., 91, 293–310, https://doi.org/10.1017/S0016774600000457, 2012.

Faber, P. A., Evrard, V., Woodland, R. J., Cartwright, I. C., and Cook, P. L.: Pore-water exchange driven by tidal pumping causes alkalinity export in two intertidal inlets, Limnol. Oceanogr., 59, 1749–1763, https://doi.org/10.4319/lo.2014.59.5.1749, 2014.

Friedlingstein, P., O'Sullivan, M., Jones, M. W., Andrew, R. M., Gregor, L., Hauck, J., Le Quéré, C., Luijkx, I. T., Olsen, A., Peters, G. P., Peters, W., Pongratz, J., Schwingshackl, C., Sitch, S., Canadell, J. G., Ciais, P., Jackson, R. B., Alin, S. R., Alkama, R., Arneth, A., Arora, V. K., Bates, N. R., Becker, M., Bellouin, N., Bittig, H. C., Bopp, L., Chevallier, F., Chini, L. P., Cronin, M., Evans, W., Falk, S., Feely, R. A., Gasser, T., Gehlen, M., Gkritzalis, T., Gloege, L., Grassi, G., Gruber, N., Gürses, Ö., Harris, I., Hefner, M., Houghton, R. A., Hurtt, G. C., Iida, Y., Ilyina, T., Jain, A. K., Jersild, A., Kadono, K., Kato, E., Kennedy, D., Klein Goldewijk, K., Knauer, J., Korsbakken, J. I., Landschützer, P., Lefèvre, N., Lindsay, K., Liu, J., Liu, Z., Marland, G., Mayot, N., McGrath, M. J., Metzl, N., Monacci, N. M., Munro, D. R., Nakaoka, S.-I., Niwa, Y., O'Brien, K., Ono, T., Palmer, P. I., Pan, N., Pierrot, D., Pocock, K., Poulter, B., Resplandy, L., Robertson, E., Rödenbeck, C., Rodriguez, C., Rosan, T. M., Schwinger, J., Séférian, R., Shutler, J. D., Skjelvan, I., Steinhoff, T., Sun, Q., Sutton, A. J., Sweeney, C., Takao, S., Tanhua, T., Tans, P. P., Tian, X., Tian, H., Tilbrook, B., Tsujino, H., Tubiello, F., van der Werf, G. R., Walker, A. P., Wanninkhof, R., Whitehead, C., Willstrand Wranne, A., Wright, R., Yuan, W., Yue, C., Yue, X., Zaehle, S., Zeng, J., and Zheng, B.: Global Carbon Budget 2022, Earth Syst. Sci. Data, 14, 4811–4900, https://doi.org/10.5194/essd-14-4811-2022, 2022.

Glavovic, B., Limburg, K., Liu, K., Emeis, K., Thomas, H., Kremer, H., Avril, B., Zhang, J., Mulholland, M., and Glaser, M.: Living on the Margin in the Anthropocene: engagement arenas for sustainability research and action at the ocean–land interface, Curr. Opin. Env. Sust., 14, 232–238, https://doi.org/10.1016/j.cosust.2015.06.003, 2015.

Grasshoff, K., Kremling, K., and Ehrhardt, M.: Methods of seawater analysis, John Wiley & Sons, ISBN 978-3-527-61399-1, 2009.

Hansen, H. and Koroleff, F.: Determination of nutrients. Methods of Seawater Analysis: Third, Completely Revised and Extended Edition, edited by: Grasshoff, K., Kremling, K., and Ehrhardt, M., Wiley-VCH Verlag GmbH, Weinheim, Germany, https://doi.org/10.1002/9783527613984.ch10, 2007.

Hickel, W.: Seston in the Wadden Sea of Sylt (German Bight, North Sea), Netherlands Institute for Sea Research – Publication Series, 10, 113–131, 1984.

Hoppema, J.: The distribution and seasonal variation of alkalinity in the southern bight of the North Sea and in the western Wadden Sea, Neth. J. Sea Res., 26, 11–23, https://doi.org/10.1016/0077-7579(90)90053-J, 1990.

Hoppema, J.: The oxygen budget of the western Wadden Sea, The Netherlands, Estuar. Coast. Shelf S., 32, 483–502, https://doi.org/10.1016/0272-7714(91)90036-B, 1991.

Hoppema, J.: Carbon dioxide and oxygen disequilibrium in a tidal basin (Dutch Wadden Sea), Neth. J. Sea Res., 31, 221–229, https://doi.org/10.1016/0077-7579(93)90023-L, 1993.

Hu, X. and Cai, W. J.: An assessment of ocean margin anaerobic processes on oceanic alkalinity budget, Global Biogeochem. Cy., 25, GB3003, https://doi.org/10.1029/2010GB003859, 2011.

Huettel, M., Røy, H., Precht, E., and Ehrenhauss, S.: Hydrodynamical impact on biogeochemical processes in aquatic sediments, in: The Interactions between Sediments and Water. Developments in Hydrobiology, edited by: Kronvang, B., vol. 169, Springer, Dordrecht, https://doi.org/10.1007/978-94-017-3366-3_31, 2003.

Jahnke, R. A., Craven, D. B., and Gaillard, J.-F.: The influence of organic matter diagenesis on $CaCO_3$ dissolution at the deep-sea floor, Geochim. Cosmochim. Ac., 58, 2799–2809, 1994.

Jensen, K., Jensen, M., and Kristensen, E.: Nitrification and denitrification in Wadden Sea sediments (Königshafen, Island of Sylt, Germany) as measured by nitrogen isotope pairing and isotope dilution, Aquat. Microb. Ecol., 11, 181–191, https://doi.org/10.3354/ame011181, 1996.

Keith, D. W., Ha-Duong, M., and Stolaroff, J. K.: Climate strategy with CO_2 capture from the air, Climatic Change, 74, 17–45, https://doi.org/10.1007/s10584-005-9026-x, 2006.

Kérouel, R. and Aminot, A.: Fluorometric determination of ammonia in sea and estuarine waters by direct segmented flow analysis, Mar. Chem., 57, 265–275, https://doi.org/10.1016/S0304-4203(97)00040-6, 1997.

Kieskamp, W. M., Lohse, L., Epping, E., and Helder, W.: Seasonal variation in denitrification rates and nitrous oxide fluxes in intertidal sediments of the western Wadden Sea, Mar. Ecol. Prog. Ser., 72, 145–151, 1991.

Legendre, P.: lmodel2: Model II Regression, R package version 1.7-3, https://CRAN.R-project.org/package=lmodel2 (last access: 18 October 2024), 2018.

Lewis, E. R. and Wallace, D. W. R.: Program Developed for CO_2 System Calculations, United States, https://doi.org/10.15485/1464255, 1998.

Louters, T. and Gerritsen, F.: The Riddle of the Sands: A Tidal SystenVs Answer to a Rising Sea Level, report RIKZ-94.040, National Institute for Coastal and Marine management (RIKZ), ISBN 90-369-0084-0, 1994.

Marx, A., Dusek, J., Jankovec, J., Sanda, M., Vogel, T., van Geldern, R., Hartmann, J., and Barth, J. A. C.: A review of CO_2 and associated carbon dynamics in headwater streams: A global perspective, Rev. Geophys., 55, 560-585, https://doi.org/10.1002/2016RG000547, 2017.

Matthews, H. D. and Caldeira, K.: Stabilizing climate requires near-zero emissions, Geophys. Res. Lett., 35, L04705, https://doi.org/10.1029/2007GL032388, 2008.

Mehrbach, C., Culberson, C., Hawley, J., and Pytkowicx, R.: Measurement of the apparent dissociation constants of carbonic acid in seawater at atmospheric pressure, Limnol. Oceanogr., 18, 897–907, https://doi.org/10.4319/lo.1973.18.6.0897, 1973.

Meybeck, M.: Global chemical weathering of surficial rocks estimated from river dissolved loads, Am. J. Sci., 287, 401–428, https://doi.org/10.2475/ajs.287.5.401, 1987.

Middelburg, J. J., Soetaert, K., and Hagens, M.: Ocean alkalinity, buffering and biogeochemical processes, Rev. Geophys., 58, e2019RG000681, https://doi.org/10.1029/2019RG000681, 2020.

Millero, F. J., Byrne, R. H., Wanninkhof, R., Feely, R., Clayton, T., Murphy, P., and Lamb, M. F.: The internal consistency of CO_2 measurements in the equatorial Pacific, Mar. Chem., 44, 269–280, 1993.

Norbisrath, M., Pätsch, J., Dähnke, K., Sanders, T., Schulz, G., van Beusekom, J. E. E., and Thomas, H.: Metabolic alkalinity release from large port facilities (Hamburg, Germany) and impact on coastal carbon storage, Biogeosciences, 19, 5151–5165, https://doi.org/10.5194/bg-19-5151-2022, 2022.

Norbisrath, M., Neumann, A., Dähnke, K., Sanders, T., Schöl, A., van Beusekom, J. E. E., and Thomas, H.: Alkalinity and nitrate dynamics reveal dominance of anammox in a hyper-turbid estuary, Biogeosciences, 20, 4307–4321, https://doi.org/10.5194/bg-20-4307-2023, 2023.

Orr, J. C., Epitalon, J.-M., Dickson, A. G., and Gattuso, J.-P.: Routine uncertainty propagation for the marine carbon dioxide system, Mar. Chem., 207, 84–107, 2018.

Pätsch, J.: Daily Loads of Nutrients, Total Alkalinity, Dissolved Inorganic Carbon and Dissolved Organic Carbon of the European Continental Rivers for the Years 1977–2022, Uni Hamburg [data set], https://wiki.cen.uni-hamburg.de/ifm/ECOHAM/DATA_RIVER (last access: 19 October 2024), 2024.

Petersen, W., Schroeder, F., and Bockelmann, F.-D.: FerryBox-Application of continuous water quality observations along transects in the North Sea, Ocean Dynam., 61, 1541–1554, https://doi.org/10.1007/s10236-011-0445-0, 2011.

Postma, H.: Hydrography of the Dutch Wadden sea, Arch. Neerl. Zool., 10, 405–511, 1954.

R Core Team: R: A language and environment for statistical computing, R version 3.6.1 (2019-07-05), RStudio Version 1.3.1073, R Foundation for Statistical Computing, Vienna, Austria, https://www.R-project.org/ (last access: 18 October 2024), 2019.

Renforth, P. and Henderson, G.: Assessing ocean alkalinity for carbon sequestration, Rev. Geophys., 55, 636–674, https://doi.org/10.1002/2016RG000533, 2017.

Ridderinkhof, H., Zimmerman, J., and Philippart, M.: Tidal exchange between the North Sea and Dutch Wadden Sea and mixing time scales of the tidal basins, Neth. J. Sea Res., 25, 331–350, https://doi.org/10.1016/0077-7579(90)90042-F, 1990.

Røy, H., Lee, J. S., Jansen, S., and de Beer, D.: Tide-driven deep pore-water flow in intertidal sand flats, Limnol. Oceanogr., 53, 1521–1530, https://doi.org/10.4319/lo.2008.53.4.1521, 2008.

Rutgers van der Loeff, M.: Transport van reactief silikaat uit Waddenzee sediment naar het bovenstaande water, NIOZ-rapport, NIOZ Open Repository 304860, http://imis.nioz.nl/imis.php?module=ref&refid=13141&basketaction=add (last access: 21 October 2024), 1974.

Sabine, C. L., Feely, R. A., Gruber, N., Key, R. M., Lee, K., Bullister, J. L., Wanninkhof, R., Wong, C., Wallace, D. W., and Tilbrook, B.: The oceanic sink for anthropogenic CO_2, Science, 305, 367–371, https://doi.org/10.1126/science.1097403, 2004.

Santos, I. R., Chen, X., Lecher, A. L., Sawyer, A. H., Moosdorf, N., Rodellas, V., Tamborski, J., Cho, H.-M., Dimova, N., and Sugimoto, R.: Submarine groundwater discharge impacts on coastal nutrient biogeochemistry, Nature Reviews Earth & Environment, 2, 307–323, https://doi.org/10.1038/s43017-021-00152-0, 2021.

Schwichtenberg, F., Callies, U., and van Beusekom, J. E.: Residence times in shallow waters help explain regional differences in Wadden Sea eutrophication, Geo-Mar. Lett., 37, 171–177, https://doi.org/10.1007/s00367-016-0482-2, 2017.

Schwichtenberg, F., Pätsch, J., Böttcher, M. E., Thomas, H., Winde, V., and Emeis, K.-C.: The impact of intertidal areas on the carbonate system of the southern North Sea, Biogeosciences, 17, 4223–4245, https://doi.org/10.5194/bg-17-4223-2020, 2020.

Shadwick, E., Thomas, H., Gratton, Y., Leong, D., Moore, S., Papakyriakou, T., and Prowe, A.: Export of Pacific carbon through the Arctic Archipelago to the North Atlantic, Cont. Shelf Res., 31, 806–816, https://doi.org/10.1016/j.csr.2011.01.014, 2011.

Suchet, P. A. and Probst, J.-L.: Modelling of atmospheric CO_2 consumption by chemical weathering of rocks: application to the Garonne, Congo and Amazon basins, Chem. Geol., 107, 205–210, https://doi.org/10.1016/0009-2541(93)90174-H, 1993.

Thomas, H., Bozec, Y., Elkalay, K., and De Baar, H. J.: Enhanced open ocean storage of CO_2 from shelf sea pumping, Science, 304, 1005–1008, https://doi.org/10.1126/science.1095491, 2004.

Thomas, H., Schiettecatte, L.-S., Suykens, K., Koné, Y. J. M., Shadwick, E. H., Prowe, A. E. F., Bozec, Y., de Baar, H. J. W., and Borges, A. V.: Enhanced ocean carbon storage from anaerobic alkalinity generation in coastal sediments, Biogeosciences, 6, 267–274, https://doi.org/10.5194/bg-6-267-2009, 2009.

van Bennekom, A., Krijgsman-van Hartingsveld, E., van der Veer, G., and van Voorst, H.: The seasonal cycles of reactive silicate and suspended diatoms in the Dutch Wadden Sea, Neth. J. Sea Res., 8, 174–207, https://doi.org/10.1016/0077-7579(74)90016-7, 1974.

van Beusekom, J. and de Jonge, V.: Long-term changes in Wadden Sea nutrient cycles: importance of organic matter import from the North Sea, Hydrobiologia, 475, 185–194, https://doi.org/10.1023/A:1020361124656, 2002.

van Beusekom, J., Brockmann, U., Hesse, K.-J., Hickel, W., Poremba, K., and Tillmann, U.: The importance of sediments in the transformation and turnover of nutrients and organic matter in the Wadden Sea and German Bight, Deutsche Hydrografische Zeitschrift, 51, 245–266, https://doi.org/10.1007/BF02764176, 1999.

van Beusekom, J. E., Buschbaum, C., and Reise, K.: Wadden Sea tidal basins and the mediating role of the North Sea in ecological processes: scaling up of management?, Ocean Coast. Manage.,

68, 69–78, https://doi.org/10.1016/j.ocecoaman.2012.05.002, 2012.

van Beusekom, J. E., Carstensen, J., Dolch, T., Grage, A., Hofmeister, R., Lenhart, H., Kerimoglu, O., Kolbe, K., Pätsch, J., and Rick, J.: Wadden Sea Eutrophication: long-term trends and regional differences, Frontiers in Marine Science, 6, 370, https://doi.org/10.3389/fmars.2019.00370, 2019.

van der Zee, C. and Chou, L.: Seasonal cycling of phosphorus in the Southern Bight of the North Sea, Biogeosciences, 2, 27–42, https://doi.org/10.5194/bg-2-27-2005, 2005.

van Raaphorst, W. and van der Veer, H. W.: The phosphorus budget of the Marsdiep tidal basin (Dutch Wadden Sea) in the period 1950–1985: importance of the exchange with the North Sea, Hydrobiologia, 195, 21–38, https://doi.org/10.1007/BF00026811, 1990.

Voynova, Y. G., Petersen, W., Gehrung, M., Aßmann, S., and King, A. L.: Intertidal regions changing coastal alkalinity: The Wadden Sea-North Sea tidally coupled bioreactor, Limnol. Oceanogr., 64, 1135–1149, 2019.

Wang, Z. A., Kroeger, K. D., Ganju, N. K., Gonneea, M. E., and Chu, S. N.: Intertidal salt marshes as an important source of inorganic carbon to the coastal ocean, Limnol. Oceanogr., 61, 1916–1931, 2016.

Waska, H. and Kim, G.: Submarine groundwater discharge (SGD) as a main nutrient source for benthic and water-column primary production in a large intertidal environment of the Yellow Sea, J. Sea Res., 65, 103–113, https://doi.org/10.1016/j.seares.2010.08.001, 2011.

Wickham, H.: ggplot2: Elegant Graphics for Data Analysis, Springer-Verlag, New York, 2016.

Wolf-Gladrow, D. A., Zeebe, R. E., Klaas, C., Körtzinger, A., and Dickson, A. G.: Total alkalinity: The explicit conservative expression and its application to biogeochemical processes, Mar. Chem., 106, 287–300, https://doi.org/10.1016/j.marchem.2007.01.006, 2007.

Wu, Z., Zhou, H., Zhang, S., and Liu, Y.: Using ^{222}Rn to estimate submarine groundwater discharge (SGD) and the associated nutrient fluxes into Xiangshan Bay, East China Sea, Mar. Pollut. Bull., 73, 183–191, https://doi.org/10.1016/j.marpolbul.2013.05.024, 2013.

Zalasiewicz, J., Williams, M., Steffen, W., and Crutzen, P.: The new world of the Anthropocene, Environ. Sci. Technol., 44, 2228–2231, https://doi.org/10.1021/es903118j, 2010.

Zhang, C., Shi, T., Liu, J., He, Z., Thomas, H., Dong, H., Rinkevich, B., Wang, Y., Hyun, J.-H., and Weinbauer, M.: Eco-engineering approaches for ocean negative carbon emission, Sci. Bull., 67, 2564–2573, https://doi.org/10.1016/j.scib.2022.11.016, 2022.